Interspin Distances in Spin-Labeled Metmyoglobin Variants Determined by Saturation Recovery EPR

Yi Zhou, Bruce E. Bowler, Kim Lynch, Sandra S. Eaton, and Gareth R. Eaton
Department of Chemistry and Biochemistry, University of Denver, Denver, Colorado 80208-2436 USA

ABSTRACT Saturation recovery (SR) electron paramagnetic resonance was used to determine the distance between iron and nitroxyl for spin-labeled metmyoglobin variants in low-spin and high-spin states of the Fe(III). The interspin distances were measured by analyzing the effect of the heme iron on the spin-lattice relaxation rates of the nitroxyl spin label using the modified Bloembergen equation for low-spin species, and an analogue of the Bloembergen equation for high-spin species. Insight simulations of the spin-labeled protein structures also were used to determine the interspin distances. The distances obtained by SR for high-spin and low-spin complexes with 15–20 Å interspin distances, for low-spin CN^- and high-spin formate adducts at distances up to about 30 Å, and results from Insight calculations were in good agreement. For variants with 25–30 Å interspin distances, the distances obtained by SR for the fluoride adducts were shorter than observed for the CN^- or formate adducts or predicted by Insight simulations. Of the heme axial ligands examined (CN^-, imidazole, F^-, and formate), CN^- is the best choice for determination of iron-nitroxyl distances in the range of 15–30 Å.

INTRODUCTION

Electron paramagnetic resonance (EPR) of spin labels attached to proteins is a powerful tool to study protein structure and dynamics (Berliner and Reuben, 1989). Initially, spin labeling took advantage of the naturally occurring cysteines in proteins. More recently, site-directed mutagenesis has been used to introduce cysteines at desired locations in a protein (Hubbell and Altenbach, 1994). Stable nitroxyl free radicals are then attached to the cysteine residues to provide a paramagnetic probe. Due to the larger magnetic moments of unpaired electrons than of nuclei, electron-electron spin-spin interactions can be detected over longer distances than electron-nuclear or nuclear-nuclear interactions. The EPR technique required to obtain structural information in systems with two paramagnetic centers depends on the interspin distances and on electron spin relaxation times. A variety of continuous wave (CW) and pulsed techniques have been developed to determine distances in biomolecules labeled with two nitroxyl spin labels (Barnes et al., 1999; Rabenstein and Shin, 1995; Milov et al., 1998; Martin et al., 1998). In systems that contain a rapidly relaxing paramagnetic metal center, the effect of that paramagnetic center on the electron spin relaxation rate of a more slowly relaxing center can be used to determine interspin distances (Poole and Farach, 1971; Kulikov and Likhtenshtein, 1977). Early uses of the effect of a rapidly relaxing metal ion on a more slowly relaxing center to obtain interspin distances relied upon CW power saturation curves to estimate a value of T_1 in the presence and absence of the rapidly relaxing metal (for reviews see Kulikov and Likhtenshtein, 1977; Eaton and Eaton, 1988). Due to the orientation dependence of the dipolar interaction, the saturation recovery (SR) curve for the slowly relaxing partner is not a single exponential and, therefore, the interspin distance can be evaluated more accurately by examining the full shape of the SR curve (Hirsch and Brudvig, 1993; Rakowsky et al., 1995) instead of approximating it as a single exponential.

We are interested in assessing how accurately interspin distances can be obtained by analysis of long-pulse SR curves for the slowly relaxing partner in systems such as heme proteins for which the metal relaxation rate can be measured directly. In studies of spin-labeled heme porphyrins and spin-labeled hemoglobin, reasonable distances in the range of 10 to 17 Å were obtained (Budker et al., 1995; Rakowsky et al., 1995, 1998; Seiter et al., 1998). In this study we seek to extend the measurements of heme-nitroxyl distances via analysis of EPR SR curves to longer distances using variants of sperm whale myoglobin (Fig. 1). For four variants, we have examined the effect of both low-spin ($S = 1/2$) and high-spin ($S = 5/2$) heme on the relaxation rate of nitroxyl spin labels attached to cysteines at selected locations on the protein. Interspin distances are in the range of 16 to 30 Å. We have compared the utility for distance measurements of imidazole and CN^- low-spin complexes and F^- and formate high-spin complexes. The interspin distances obtained by analysis of the SR data were compared with distances calculated by molecular modeling using the Insight II software.

Received for publication 11 February 2000 and in final form 8 May 2000.
Address reprint requests to Dr. Sandra Eaton, Department of Chemistry, University of Denver, 2050 East Iliff Avenue, Denver, CO 80208. Tel.: 303-871-3102; Fax: 303-871-2254; E-mail: seaton@du.edu.

0006-3495/00/08/1039/14 $2.00

EXPERIMENTAL SECTION

Preparation of spin-labeled myoglobin

Wild-type sperm whale Mb synthetic gene carried in the vector, pMb122, was a generous gift from Sligar's lab (Phillips et al., 1990; Springer and Sligar, 1987). The gene was excised from the pMb122 vector with the restriction enzymes *Pst*I and *Kpn*I, followed by ligation between the *Pst*I

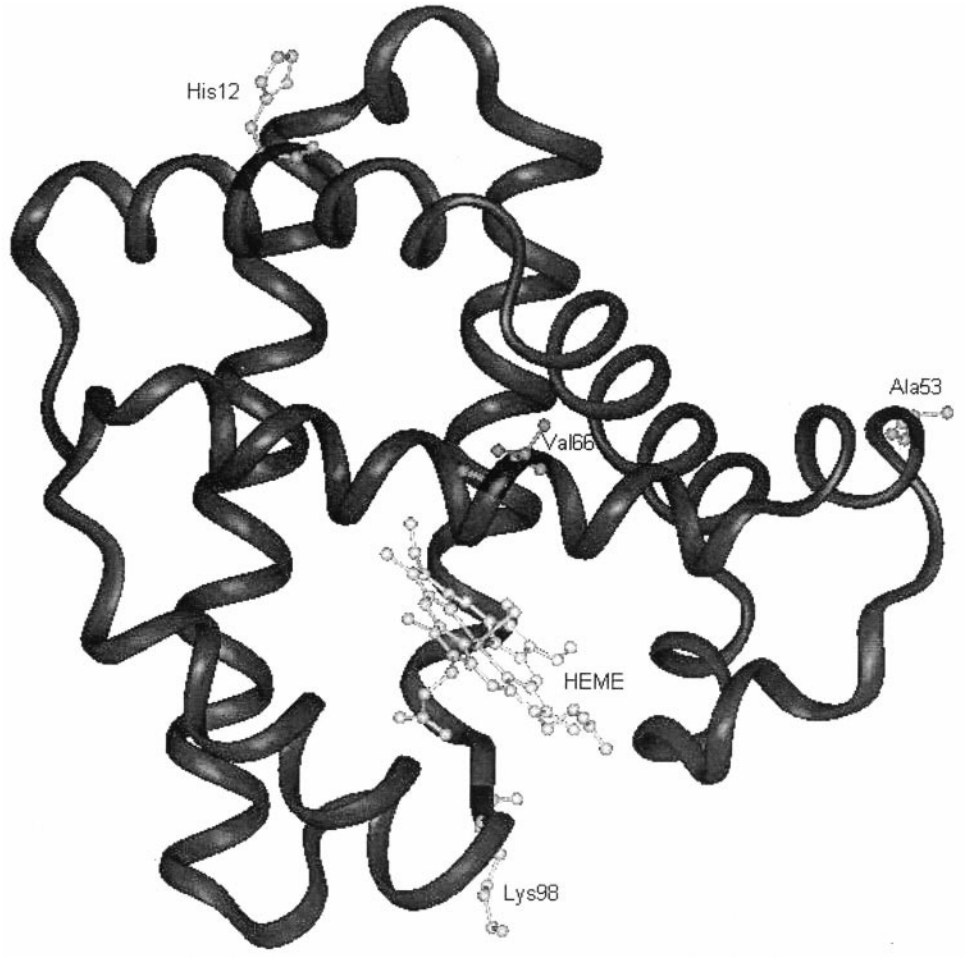

FIGURE 1 Structure of sperm whale myoglobin based on the Brookhaven Protein Data Bank pdb1mbw file. The heme and mutation sites are shown.

and *Kpn*I sites of the phagemid vector pBS(−) (Stratagene, La Jolla, CA) using standard techniques (Maniatis et al., 1992). The resulting vector, pBS/Mb, was transformed into *Escherichia coli* XL-Blue cells (Stratagene). Single-stranded DNA was generated by infection of these cells with helper phage R408 (Russel et al., 1986) and used as a template for oligonucleotide-directed mutagenesis. Variants MbV66C (notation V66C indicates that valine 66 was replaced by cysteine), MbK98C, MbH12C, and MbA53C, were prepared using the Sculptor in vitro Mutagenesis System (Amersham Pharmacia Biotech, Piscataway, NJ). The following oligonucleotides were used as mutagenesis primers: MbV66C, 5′-GAAAAAACATGGT*TGC*ACCGTGTTAAC-3′; MbK98C, 5′-GCTACTAAACAT*TGC*ATCCCGATCAAA-3′; MbH12C, 5′-GCTGGTTCTG*TGC*GTTTGGGCTA-3′; and MbA53C, 5′-TGAAAACTGAA*TGC*GAAATGAAAGC-3′ (the site of mutation is in italics in each oligonucleotide). Complete sequences of the mutant genes were verified by using the dideoxy sequencing method (Biggin et al., 1983), and the genes were transformed into TB-1 *E. coli* cells (New England Biolabs, Beverly, MA). Expression of Mb followed a modified Springer and Sligar (1987) procedure (Chen and Sligar, personal communication). A starter culture of 5 ml LB media (10 g tryptone, 5 g yeast extract, and 10 g NaCl in 1 L water) containing 200 mg/L ampicillin was grown at 37°C overnight in a 250-rpm shaker. An intermediate culture was grown for ~8 h after inoculating 65 ml of LB media with 650 μl of the starter culture. Six 2800-ml Fernbach flasks, each containing 1 L of media, were inoculated with 10 ml of the intermediate culture and grown overnight, followed by 3 to 4 h of slow shaking (100 rpm). Harvested cells were spread thinly (~2–5 mm) in a plastic bag and frozen at −80°C for at least 2 h. Typical wet cell weight was 25 to 35 g. In the following paragraphs, Mb is used as a generic abbreviation for wild-type and variants of myoglobin.

Cell lysis was performed by the Springer and Sligar (1987) procedure, except that the dithiothreitol (DTT; Sigma, St. Louis, MO) concentration was increased from 0.5 mM to 5 mM in the MbH12C preparation to prevent auto-oxidation, and in the MbA53C preparation to prevent dimerization. Lysate was spun down at 13.5K rpm in an ss34 rotor (Dupont) for 30 min. The supernatant was collected and adjusted to pH 6.0 with 50 mM NaH_2PO_4, and then diluted four- to fivefold with cold distilled deionized water. This solution was refrigerated at 4°C for 2 h, centrifuged in a GSA rotor for 30 min at 10K rpm, and batch-loaded onto ~20 ml of CM Sepharose resin (Amersham Pharmacia). In later preparations of MbH12C and MbA53C, immediate filtration through a 0.4-μm filter was used instead of the refrigeration and centrifugation step. The Mb-loaded resin was then placed on top of an approximately 80 ml bed-volume column (3 × 20 cm, glass) of CM-Sepharose resin. Mb was eluted using a linear gradient from 10 mM NaH_2PO_4, 1 mM EDTA (pH 6.0) to 30 mM Na_2HPO_4 (pH ~9.0). Mb fractions eluted at about pH 7.0. When preparing MbH12C and MbA53C, 5 mM freshly prepared DTT was added to all chromatography buffers to decrease oxidation of the Fe(II) heme or dimerization via disulfide formation. Mb-containing fractions were combined and run through a G-50 superfine (Amersham Pharmacia) column (~80 ml bed volume, 1.7 × 40 cm, glass) in 20 mM Tris-HCl, 1 mM EDTA (pH 8.4) buffer. Fractions with ratios of the absorbance of the Soret band (typically 415–417 nm as a result of a mixture of OxyMb and MetMb) to that of the protein band (280 nm) higher than 3.2 were collected. Sodium dodecyl sulfate-polyacrylamide gel electrophoresis showed that Mb frac-

tions with this ratio were homogeneous. In preparing MbH12C and MbA53C, DTT was removed with a Sephadex G-25 (medium) column (~45 ml bed volume) before spin labeling. Cysteine was assayed with 5,5′-dithio-bis(2-nitrobenzoic acid) (Sigma) (Zuniga and Nall, 1983; Habeeb, 1972), confirming that there was one cysteine on each metMb molecule. Typical yield was ~1 mg Mb/g wet cells.

Spin labeling with 4-(2-iodoacetamido)-TEMPO (Sigma) to form metMb-SL followed the procedure of Manoharan et al. (1990) with some modification. The labeling reaction lasted either 1 h at room temperature followed by overnight refrigeration or 2 h at room temperature. In the second preparation of MbA53C-SL, the protein concentration was decreased from 1 mM to ~0.2 mM to decrease the dimerization rate. 1.5 molar equivalent $K_3Fe(CN)_6$ was added to oxidize oxyMb-SL to metMb-SL, and excess oxidant was removed together with free spin label by passing the sample through a Sephadex G-25 column (~45 ml bed volume) equilibrated to 30 mM potassium phosphate buffer, pH 6.8, immediately after adding the $K_3Fe(CN)_6$. Protein was stored in 30 mM potassium phosphate buffer, pH 6.8, and its concentration was determined by the intensity of the Soret band (409 nm, $\epsilon = 1.57 \times 10^5$ $cm^{-1}M^{-1}$; Antonini and Brunori, 1971). The concentration of spin label in metMb-SL was determined by double integration of the room temperature CW EPR spectrum of the nitroxyl signal and comparison with the double integral of spectra of known concentrations of 4-oxo-2,2,6,6-tetramethylpiperidin-1-oxyl (TEMPONE) in water. Labeling efficiency was 70–100%.

Horse heart Mb (metHHMb) was used as a model to estimate the ligand dissociation constants and molar absorptivities for sperm whale Mb variants. Titration of CN^-, Im^-, and F^- into Mb solutions was monitored using UV-Vis spectroscopy. The Mb concentration before titration was determined by the intensity of the Soret band (408 nm, $\epsilon = 1.88 \times 10^5$ $cm^{-1}M^{-1}$; Antonini and Brunori, 1971). Molar absorptivities and ligand dissociation constants are consistent with literature values for sperm whale myoglobin (Table 1). Values of K_D were used as a guide to determine concentrations of ligands in preparing samples for EPR experiments. CN-metMb-SL was prepared by addition of KCN solution to produce a 3:1 ratio of CN^- to Mb. Samples of CN-metMb-SL were handled quickly in a cold room to minimize destruction of the spin label (Budker et al., 1995). Im-metMb-SL was prepared by addition of pH 6.8 imidazole solution to give a final imidazole concentration of 200 mM. F-metMb-SL was prepared by addition of pH 6.8 KF solution to give a final F^- concentration of 100 mM. EPR samples were diluted with glycerol to give 1:1 H_2O:glycerol (v/v) solutions, and frozen immediately in liquid nitrogen. Formate-metMb-SL was prepared differently due to the low binding constant for formate to heme iron, $K_a = 1.0 \times 10^1$ (Leci et al., 1995; Aime et al., 1996), and the fact that Mb precipitates at high formate concentrations. A 1:1 (v/v) mixture of aqueous 6 M sodium formate/formic acid pH 7.0 and glycerol was added to metMb-SL and the solution was concentrated in an Ultrafree-0.5 concentrator (Millipore, Bedford, MA). This step was repeated several times to change the buffer from phosphate to formate. EPR samples had a protein concentration in 1:1 H_2O:glycerol solution of 0.5–1.0 mM. Samples were degassed by several freeze-pump-thaw cycles followed by back-filling with helium immediately before EPR experiments.

Preparation of Zn-MbV66C-SL

Purified MbV66C was used to make apoprotein by the acidic methyl ethyl ketone extraction method (Teale, 1959). The aqueous layer containing apoMb was diluted 10-fold with water and then concentrated to 1–2 ml in a Centriprep–10 concentrator (Millipore). A Sephadex G-25 column (~45 ml bed volume) equilibrated with water was used to remove residual methyl ethyl ketone from the concentrated aqueous phase. UV-Vis spectroscopy (280 nm $\epsilon = 15.8$ cm^{-1} mM^{-1}; Stryer, 1965) was used to determine the yield of apoMb. The crude apoMb was dialyzed against 20 mM Tris-HCl, 1 mM EDTA (pH 8.4) buffer for at least 6 h, and a small amount of precipitate was removed by centrifugation. The apoMb was spin labeled as described above. Zn-porphyrin reconstitution was performed using a modification of literature procedures (Scholler et al., 1978; Leonard et al., 1974; Axup et al., 1988). Five equivalents of Zn-protoporphyrin IX were added to a minimum amount of 0.1 N NaOH (~2 mg/ml) and vortexed for at least 30 min in the dark. The solution was centrifuged to remove any suspended solids and added dropwise to a solution of apoMb-SL (0.5 to 1 mg/ml) in 30 mM sodium phosphate (pH 6.8). The pH was monitored and adjusted with the same buffer to prevent it from going above 9.0. The mixture was stirred overnight in the dark, the pH was adjusted to 6.0 with 50 mM NaH_2PO_4, and the solution was diluted fourfold with water. The dilute solution was loaded onto a CM-Sepharose column (~100 ml bed volume, 3 × 20 cm glass column) equilibrated with 10 mM NaH_2PO_4, pH 6.0, buffer. After washing with 1 bed volume of buffer to remove Zn-porphyrin and apoMb-SL, Zn-Mb-SL was eluted with 20 mM Tris-HCl, 1 mM EDTA (pH 8.4) buffer. Fractions with Abs(427 nm)/Abs(280 nm) $\geq$ 8 were collected and concentrated, and an equal volume of glycerol was added. To check the effect of high salt concentrations on the spin-lattice relaxation of the spin label, Zn-MbV66C-SL in 3 M formate buffer was prepared using the buffer replacement method described above.

CW EPR spectra

Microslides (0.4 mm path length; VitroCom, Rockaway, NJ) were used for room temperature spectra. Quartz tubes (4.0 mm outside diameter) were used for liquid nitrogen and liquid helium spectroscopy. CW EPR spectra at room temperature or liquid nitrogen temperatures were obtained on a Varian E9 spectrometer with a TE_{102} rectangular resonator and 100 kHz magnetic field modulation. Spectra at liquid helium temperatures were obtained on a Bruker ESP380E spectrometer operating at 9.2 GHz with a split ring resonator and an Oxford CF935 cryostat. Spectra were obtained

TABLE 1 Binding of axial ligands to metmyoglobin

complex	ε (cm^{-1} mM^{-1}), (λ_{max}) pH 8.4	K_D (M)*	Literature values of ε (cm^{-1} mM^{-1}),† (λ_{max}), pH 7	Literature values of K_D (M)‡
CN-metMb	8.7 (542 nm)	5×10^{-6}	10.7 (540 nm) Hanania et al., 1966	1.3×10^{-6}, Dou et al., 1996
Im-metMb	8.8 (536 nm)	4.5×10^{-3}		0.022, pH 8.0, Mansy et al., 1998
F-metMb	6.6 (605 nm)	1.6×10^{-3}	7.82 (609 nm) Hanania et al., 1966	(crystal) 0.013–0.017, Conti et al., 1993; Aime et al., 1996
Formate-met Mb (crystal)			—	0.1; Leci et al., 1995; Aime et al., 1996

*Values of K_D were obtained for horse heart myoglobin (Sigma) by titration.

†For sperm whale myoglobin.

‡For ease of comparison, when the association constant, K_a, was reported, it was converted to K_D for inclusion in this table.

with microwave powers that produced signals in the linear-response regime.

Pulsed EPR measurements of iron relaxation rates

For low-spin Fe(III), values of $1/T_1$ were obtained by long-pulse saturation recovery on a Bruker ESP380E spectrometer with a split-ring resonator at 5–13 K for CN-metMb and at 6–15 K for Im-metMb, and by 3-pulse inversion recovery at 5–17 K for CN-metMb, at 12–28 K for Im-metMb, at 4.8 -7 K for F-metMb and at 4.7–6 K for formate-metMb. Experimental data were fitted to a single exponential using a nonlinear least-squares algorithm. There were some deviations from a single exponential that may be due to a distribution in relaxation rates. Relaxation rates obtained by saturation recovery and inversion recovery were in good agreement.

SR measurements of nitroxyl relaxation rates

A locally constructed spectrometer and a TE_{102} rectangular resonator were used for the SR measurements (Quine et al., 1992). Temperatures between 16 and 70 K were obtained with liquid helium and an Oxford ESR900 flow cryostat. Temperatures between 70 and 170 K were obtained with a Varian liquid-nitrogen-cooled gas flow system. The temperatures at the sample as monitored on the ITC601 variable temperature controller readout were calibrated by replacing the sample with a tube containing a thermocouple immersed in 1:1 H_2O:glycerol. Between 10 and 70 K, the temperature at the sample is strongly dependent upon the helium flow rate, which causes as much as 2 K uncertainty in temperature. Between 90 and 170 K the uncertainty in temperature is <1 K. The effects of spectral diffusion were monitored by measuring the saturation recovery time constant as a function of the length of the saturating pulse. The data were obtained in the limit where the saturation recovery time constant is independent of the length of the pump pulse. Pump times were typically 400 μs to 1 ms. Recovery curves were signal averaged 2000 to 32,768 times in a LeCroy 9400 digital oscilloscope or an EG&G (Princeton, NJ) 9825 digitizer. All EPR data were obtained at ~9.1 to 9.2 GHz.

Insight II simulations

Insight II software (Molecular Simulations, Inc., San Diego, CA) was used to model the structures of the spin-labeled myoglobin variants. X-ray crystallographic structures of sperm whale myoglobin were downloaded from the Brookhaven Protein Data Bank: pdb1mbw (Phillips et al., 1990) for H_2O-metMb and pdb1mbi (Lionetti et al., 1991) for Im-metMb. Structures with other ligands in the heme sixth position, CN^-, F^-, and formate, were modeled based on the pdb1mbw file. The heme Fe(I) oxidation state was used to preserve the charge symmetry of the porphyrin. The nitroxyl radical N-O group was modeled as a partial double bond. Three different solvent environments were used: without solvent box, with 5 Å water box, and with 10 Å glycerol box. Charges and potentials of all atoms in the system were assigned with the extensible systematic force field. Simulations started with a crude energy minimization, followed by a dynamics simulation sampling 800 out of 8,000 conformations in a canonical ensemble at 300 K. Multi-step energy minimization with final maximal derivatives less than 0.2 kcal/mol-Å gave the stable minimized conformations. All bonds and angles in the protein structure were allowed to vary in the dynamic simulations. In the multiple-step minimization, atom displacement initially was restrained by a tethering force, which was gradually relaxed to zero. Iron-nitroxyl interspin distances were calculated as an average of distances measured from Fe to N and Fe to O coordinates. Protocols were validated by reproducibility checks. Maximum variations in interspin distance less than 0.5 Å and 0.2 Å between repeated trials were considered adequate for dynamic simulation and energy minimization, respectively.

Analysis of experimental data

Analysis of CW lineshapes to determine Fe(III) relaxation rates

The linewidths of the Fe(III) signals are temperature-dependent above ~15 K for high-spin Fe(III), above ~35 K for CN-metMb and above ~60 K for Im-metMb. The CW spectra of the high-spin Fe(III) complexes at 5 K and of the low-spin Fe(III) complexes at 15 K were analyzed with the locally written program SATMON (Rakowsky et al., 1998). The low temperature linewidths were modeled as Gaussian distributions of T_2-determined spin packets that are narrow relative to the distribution width. The widths of the Gaussian distributions, in G, for the various samples, listed in the order *x, y, z*, are: CN^-, 800, 200, 47–60; Im, 200–250, 35–40, 50–75; F^-, 15–20, 13–17, 12.5; formate, 12–20, 12–26, 7.2. The ranges of values indicate differences between variants. In the spectra of F-metMb fluorine hyperfine coupling of 42 cm^{-1} was resolved at the $g' = 2$ turning point, which is in good agreement with ENDOR data for F-metHb (Fann et al., 1995). Unresolved fluorine hyperfine of 20–24 cm^{-1} was used to simulate the perpendicular region of the spectrum, consistent with ENDOR data for F-metHb (Fann et al., 1995). It was assumed that the distribution widths and g values are independent of temperature. In the temperature range where linewidths are temperature-dependent, the iron T_2 was determined from the temperature-dependent contribution to the linewidth (Rakowsky et al., 1998) and the assumption was made that $T_1 = T_2$. For the high-spin iron porphyrins and heme proteins, the relaxation rate at 5 K is orientation-dependent, but rates at temperatures above ~15 K are not orientation-dependent (Rakowsky et al., 1998; Seiter et al., 1998).

Although excess ligand was added with the intent of converting all of the heme to a particular spin state, the conversions were not complete. There were some low-spin species in high-spin samples and some high-spin species in low-spin samples. The locally written program MONMER (Rakowsky et al., 1998) was used to simulate the CW spectra at 15 K as mixtures of two components with weightings adjusted to match the spectra. The high-spin complexes were simulated with fictitious $S' = 1/2$. The relative weightings of the two components would reflect the relative concentrations if all of the high-spin Fe(III) were in the $m_s = \pm 1/2$ levels. The zero-field splitting D for F-metMb has been reported as 6.1 cm^{-1} (Scholes et al., 1971) to 6.4 cm^{-1} (Oganesyan and Sharonov, 1998). The value of D for formate-metMb was estimated as 8.5 cm^{-1} because the iron electron spin relaxation rates are slightly slower than for aquo-metHb, which has D in the range of 8 to 11 cm^{-1} (Seiter et al., 1998). Using these values of D, the fractions of the Fe(III) in the $m_s = \pm 1/2$ levels for F-metMb and formate-metMb are about 75% and 85%, respectively, at 15 K. The calculated ratios of concentrations for high-spin and low-spin Fe(III) were corrected to account for the populations of the other m_s levels. The calculated populations are quite sensitive to the accuracy of fits to the lineshapes, so there are significant uncertainties in the resulting values. However, they provide useful estimates of the relative concentrations.

Temperature dependence of nitroxyl and Fe(III) spin-lattice relaxation rates

In the absence of interaction with a rapidly relaxing paramagnetic center, T_1 for nitroxyl radicals is longer when the external magnetic field is along the g_z axis and shorter when the magnetic field is in the *x, y* plane (Du et al., 1995). Data for a doped single crystal and for a glassy sample indicated that the orientation dependence of $1/T_1$ was approximately linear in $\sin^2\theta$, where θ is the angle between the external magnetic field and the nitroxyl g_z axis (Du et al., 1995). The SR experiments for Zn-Mb-SL and L-metMb-SL were performed with a critically coupled resonator with Q ~

3000, so only a narrow band of resonant energies is excited and observed in the experiment. However, that band of frequencies encompasses a relatively wide range of orientations of the nitroxyl because unresolved proton hyperfine splittings blur out the orientation selection of the experiment. The linewidths of the nitroxyl signals in CW spectra at low temperature are about 10 G. The SR curves for Zn-MbV66C-SL were simulated assuming a random distribution of orientations of the spin label, but only those orientations that are at resonance within a 10-gauss band centered at the experimental magnetic field were included in the simulated SR curve. An orientation selection bandwidth of 8 gauss gave similar results. In the simulations the T_1 along the g_z axis was 3.7 times the value of T_1 in the perpendicular plane.

The temperature-dependent nitroxyl relaxation rates in the perpendicular plane are similar for 1.1 mM Zn-MbV66C-SL in 1:1 H_2O:glycerol and for 0.4 mM Zn-MbV66C-SL in 1:1 H_2O:glycerol containing 3 M formate. The relaxation rates as a function of temperature were fitted to Eq. 1 (Zhou et al., 1999). The temperature dependence between 14 and 148 K is consistent with a dominant Raman process with a Debye temperature of 82 K. The coefficient, A_{Ram}, was $2.0 \times 10^4\ s^{-1}$ in 1:1 H_2O:glycerol and $2.2 \times 10^4\ s^{-1}$ in 1:1 H_2O:glycerol containing 3 M formate. An additional process makes a small contribution at higher temperatures and was modeled as a local mode with a characteristic energy of 450 K (Zhou et al., 1999).

$$\frac{1}{T_1} = A_{dir}T + A_{Ram}\left(\frac{T}{\theta_D}\right)J_8\left(\frac{\theta_D}{T}\right) + A_{loc}\left[\frac{e^{\Delta_{loc}/T}}{(e^{\Delta_{loc}/T}-1)^2}\right] + A_{Orb}\left[\frac{\Delta_{Orb}^3}{e^{\Delta_{Orb}/T}-1}\right] + A_{therm}\left[\frac{2\tau_c}{1+\omega^2\tau_c^2}\right] \quad (1)$$

where T is temperature in Kelvin, A_{dir} is the coefficient for the contribution from the direct process, A_{Ram} is the coefficient for the contribution from the Raman process, θ_D is the Debye temperature, J_8 is the transport integral,

$$J_8\left(\frac{\theta_D}{T}\right) = \int_0^{\theta_D/T} x^8 \frac{e^x}{(e^x-1)^2}\,dx,$$

A_{loc} is the coefficient for the contribution from a local vibrational mode, Δ_{loc} is the energy for the local mode in units of Kelvin, A_{Orb} is the coefficient for the contribution from the Orbach process, Δ_{Orb} is the energy separation between the ground state and the excited state for the Orbach process, A_{therm} is the coefficient for the thermally activated process $= \tau_c^0 e^{E_a/T}$, E_a is the activation energy for the thermally activated process, τ_c^0 is the pre-exponential factor, and ω is the Zeeman frequency.

The temperature dependence of T_1 for low-spin Fe(III) obtained from a combination of saturation recovery and inversion recovery at low temperatures and from CW linewidths at higher temperatures was fitted to Eq. 1 (Zhou et al., 1999). Within experimental uncertainty there was no difference in the iron relaxation rates between variants, and spin labeling had no impact on the iron relaxation rate. A contribution from the direct process dominated near 5–6 K, the Raman process dominated between ~6 and 25 K, and a thermally activated process dominated at higher temperatures. The experimental data points for the iron and nitroxyl relaxation times were often obtained at different temperatures. The fit functions obtained with Eq. 1 for Zn-MbV66C-SL and for low-spin Fe(III) were used to interpolate the relaxation rates required for the MENOSR simulations described in the following section.

Measurements of high-spin Fe(III) relaxation rates are more complicated. Due to the large zero-field splittings for F-metMb and formate-metMb, only the transitions between the $m_s = \pm 1/2$ energy levels are observed at X-band. Transitions involving $m_s = \pm 3/2$ and $m_s = \pm 5/2$ are not observed. The temperature dependence of the relaxation rates obtained for the $m_s = \pm 1/2$ transitions (Fig. 2) is consistent with Orbach processes involving excited states at 2 D and 6 D (Zhou et al., 2000). When the model

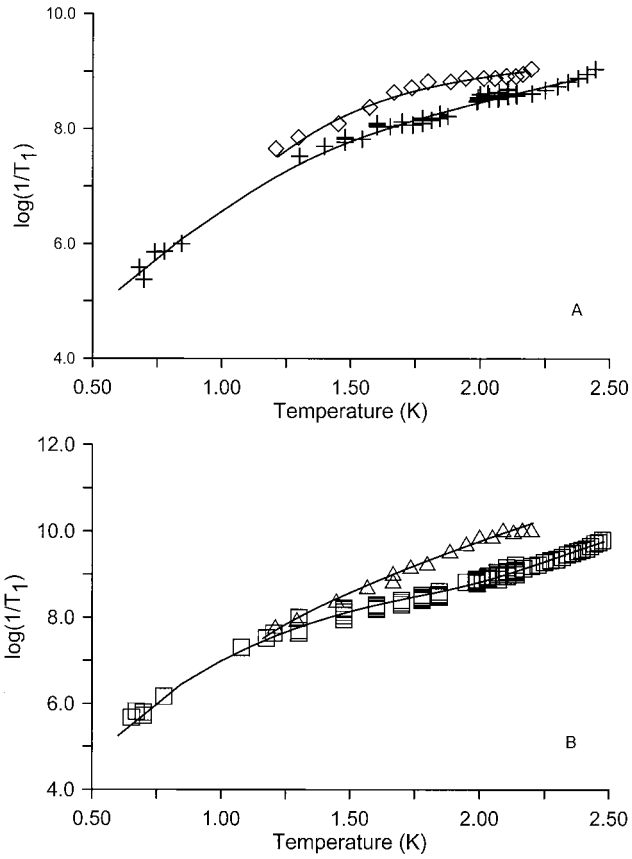

FIGURE 2 Temperature dependence of electron spin relaxation rates, $1/T_1$, for high-spin Fe(III). (A) (+) F-metMb including wild-type and several of the spin-labeled variants, based on inversion recovery and analysis of linewidths in CW spectra, *solid* fit line obtained with $A_{orb} = A_{orb2} = 1.9 \times 10^3\ s^{-1}K^{-3}$; $\Delta_{orb} = 14$ K, $A_{loc} = 4.5 \times 10^9\ s^{-1}$ and $\Delta_{loc} = 1000$ K; (◇) effective iron relaxation rates for F-metMbK98C-SL based on values required to fit the nitroxyl SR curves assuming interspin distance = 19 Å, *solid* fit line obtained with $A_{orb} = 3.0\times 10^3\ s^{-1}K^{-3}$, $A_{orb2} = 4.7 \times 10^2\ s^{-1}K^{-3}$; $\Delta_{orb} = 16$ K. (B) (□) formate-metMb including wild type and several of the spin-labeled variants, based on inversion recovery and analysis of linewidths in CW spectra, *solid* fit line obtained with $A_{orb} = 6.4 \times 10^3\ s^{-1}K^{-3}$, $A_{orb2} = 1.1\times 10^3\ s^{-1}K^{-3}$; $\Delta_{orb} = 23$ K, $A_{loc} = 2.9\times 10^{10}\ s^{-1}$ and $\Delta_{loc} = 700$ K; (△) effective iron relaxation rates for formate-metMbK98C-SL based on values required to fit the nitroxyl SR curves assuming interspin distance = 19 Å, *solid* fit line obtained with $A_{orb} = 1.0\times 10^3\ s^{-1}K^{-3}$, $A_{orb2} = 2.0 \times 10^3\ s^{-1}K^{-3}$; $\Delta_{orb} = 20$ K, $A_{loc} = 1.2 \times 10^{10}\ s^{-1}$ and $\Delta_{loc} = 500$ K.

described below was used to calculate iron-nitroxyl distances based only on the relaxation times observed for the $m_s = \pm 1/2$ energy levels, the calculated distances are shorter by 13% at shorter distances and up to 33% at longer distances than the distances obtained for low-spin complexes of the same variants, which we attribute to systematic errors in the high-spin Fe(III) relaxation rates. However, it is expected that the relaxation rates will be faster for transitions involving $m_s = \pm 3/2$ and $\pm 5/2$ than for $m_s = \pm 1/2$ (Rubenstein et al., 1971). Lacking data for these unobserved transitions, we used high-spin metMbK98C-SL complexes as a reference to estimate the effective iron relaxation rates. Based on results obtained for the low-spin analogs and on the results of the Insight II calculations, it was assumed that the interspin distance was 19 Å for metMbK98C-SL. The iron relaxation rates were then adjusted to fit the SR curves, calculated using

Eq. 3, to the experimental data for the interacting nitroxyl radical. The resulting effective iron relaxation rates (Fig. 2) are faster than the rates determined from the observed transitions by a factor of about three for fluoride and six for formate.

By either method of estimating the high-spin Fe(III) relaxation rates, the rates are faster for the formate complexes than for the fluoride complexes (Fig. 2). Part of this difference is likely to be due to differences in zero-field splitting. However, the mobility of the axial ligand may also be a factor. According to x-ray crystallographic and ^{1}H-NMR relaxometric studies (Aime et al., 1993, 1996), the fluoride is hydrogen bonded to both the distal His and to a water molecule that significantly interacts with the same His. Hydrogen bonding of formate to distal His is similar to fluoride, but there is not a hydrogen-bonded water in the formate complex (Aime et. al., 1996).

Analysis of nitroxyl SR data to obtain interspin distances

The effect of a rapidly relaxing electron spin on the spin-lattice relaxation rate for a slowly relaxing partner was described by Bloembergen (Bloembergen et al., 1959; Kulikov and Likhtenshtein, 1977). We proposed a modification to give the correct limiting behavior of the B term when $\omega_f - \omega_s$ approaches zero (Budker et al., 1995; Rakowsky et al., 1998) as shown in Eq. 2:

$$\frac{1}{T_{ls}} = \frac{1}{T_{ls}^0} + S(S+1)\left[\underbrace{\frac{b^2 T_{2f}}{1+(\omega_f-\omega_s)^2T_{2f}^2 + b^2T_{lf}T_{2f}}}_{\text{B term}} + \underbrace{\frac{c^2T_{lf}}{1+\omega_s^2T_{lf}^2}}_{\text{C term}} + \underbrace{\frac{e^2T_{2f}}{1+(\omega_f+\omega_s)^2T_{2f}^2}}_{\text{E term}}\right]$$

$$b^2 = \frac{8}{3}\left[-\frac{J}{2} - \frac{1}{4}g_s g_f \beta^2 \frac{(1-3\cos^2\theta)}{\hbar r^3}\right]^2 \quad (2)$$

$$c^2 = 3g_s^2 g_f^2 \beta^4 \frac{\sin^2\theta\cos^2\theta}{\hbar^2 r^6}$$

$$e^2 = \frac{3}{2}g_s^2 g_f^2 \beta^4 \frac{\sin^4\theta}{\hbar^2 r^6}$$

where f and s denote the fast- and slow-relaxing spins, respectively, T_{1s}^0 is T_1 for the slow-relaxing spin in the absence of spin-spin interaction, T_{1s} is T_1 for the slow-relaxing spin perturbed by the fast-relaxing spin, S is the electron spin on the fast-relaxing center, ω_f and ω_s are the resonant frequencies for the fast- and slow-relaxing spins, respectively, r is the interspin distance, and θ is the angle between the interspin vector and the external magnetic field.

Although Eq. 2 typically is written in the form including the factor of S(S+1), its derivation is based on the matrix elements and raising and lowering operators for S = 1/2. Its application to systems with S > ½ is an approximation. Consideration of the full 12 × 12 matrix for dipolar and exchange interaction between centers with S = 5/2 and S = 1/2 for the case where D is much greater than the EPR quantum, gives Eq. 3. This equation explicitly takes account of the dependence of the energy separation between the resonance for the metal and the radical on zero-field splitting D and the dependence of each term on the populations of individual m_s levels of the S = 5/2 ion. Although it is expected that T_{1f} and T_{2f} will be different for different values of m_s, we do not have experimental access to these values, so the equation is expressed in terms of effective values of T_{1f} and T_{2f}.

$$\frac{1}{T_{ls}} = \frac{1}{T_{ls}^0} + b^2\left[\frac{10(P_5+P_3)T_{2f}}{1+(4D-\omega_s)^2T_{2f}^2} + \frac{16(P_3+P_1)T_{2f}}{1+(2D-\omega_s)^2T_{2f}^2} + \frac{18P_1T_{2f}}{1+(\omega_f-\omega_s)^2T_{2f}^2}\right] + c^2\left[\frac{(25P_5+9P_3+4P_1)T_{lf}}{1+\omega_s^2T_{lf}^2} + \frac{5(P_5+P_3)T_{lf}}{1+(4D)^2T_{lf}^2} + \frac{8(P_3+P_1)T_{lf}}{1+(2D)^2T_{lf}^2} + \frac{9P_1T_{lf}}{1+\omega_f^2T_{lf}^2}\right] + e^2\left[\frac{10(P_5+P_3)T_{2f}}{1+(4D+\omega_s)^2T_{2f}^2} + \frac{16(P_3+P_1)T_{2f}}{1+(2D+\omega_s)^2T_{2f}^2} + \frac{18P_1T_{2f}}{1+(\omega_f+\omega_s)^2T_{2f}^2}\right] \quad (3)$$

where P_5, P_3, and P_1 are populations of $m_s = \pm5/2$, $\pm3/2$, and $\pm1/2$ energy levels of the S = 5/2 manifold, respectively, and other variables have the same meanings as in Eq. 2. The calculations of P_5, P_3, and P_1 assume that the Zeeman interaction is negligible compared to the zero-field splitting.

Simulations of nitroxyl SR curves based on Eqs. 2 and 3 for interaction with low- and high-spin Fe(III), respectively, were performed with a locally written program, MENOSR (Rakowsky et al., 1995). The calculations assumed a random distribution of molecules in the external magnetic field, but only those for which the nitroxyl resonance occurred within a band of 10 G centered at the magnetic field used for the experiment were included in the calculation. The g values for low-spin Fe(III) were taken from the CW simulations. For high-spin Fe(III), effective g values were used to calculate ω_f for the $m_s = \pm1/2$ transitions. The zero field splitting used for F-metMb was 6.4 cm^{-1} (Oganesyan and Sharonov, 1998), and for Formate-metMb was estimated to be 8.5 cm^{-1}, as described above. Values of T_{1s}^0 (including orientation dependence) and T_{1f} were taken from the fit functions for the temperature dependence of relaxation for Zn-Mb-SL and iron, respectively. At low temperatures electron spin echo decay constants, T_m, for the heme Fe(III) are of the order of 1 μs. Precise values of T_m are difficult to determine because of deep echo envelope modulation due to interaction with the coordinated nitrogens. A variety of processes other than T_2 can contribute to echo dephasing (Zecevic et al., 1998). However, T_2 must be at least as long as T_m so at low temperature T_2 must be greater than about 1 μs. At the temperatures where the iron had significant impact on the nitroxyl T_1, T_{1f} is much shorter than 1 μs, so it was assumed that T_{1f} was driving T_{2f} and that $T_{1f} = T_{2f}$. At the long interspin distances of these samples, it seems reasonable to assume that the contribution of electron-electron exchange is negligible compared to dipolar interaction. For initial calculations, the angle between the interspin vector and the heme *z* axis and the projection on the heme plane were both set to 45°. Subsequent calculations were performed to determine the sensitivity of the estimated distance to the orientation of the interspin vector. The value of r was adjusted to fit the nitroxyl SR data (Figs. 3-6). Plots of the difference between calculated and experimental data (Figs. 3–6) show that there are systematic deviations, which are the subject of ongoing investigations.

The calculated interspin distances for the range of temperatures at which the effects of the iron on the nitroxyl T_1 were significant are summarized in Tables 2 and 3. SR data were used for distance determinations only at temperatures where interaction with the iron caused more than a 15% change in the nitroxyl T_1. The uncertainties listed in Tables 2 and 3 are the standard deviations for the distances calculated from SR data at multiple points within the temperature ranges listed. To check the contribution of temperature uncertainty to uncertainties in the interspin distances, calcu-

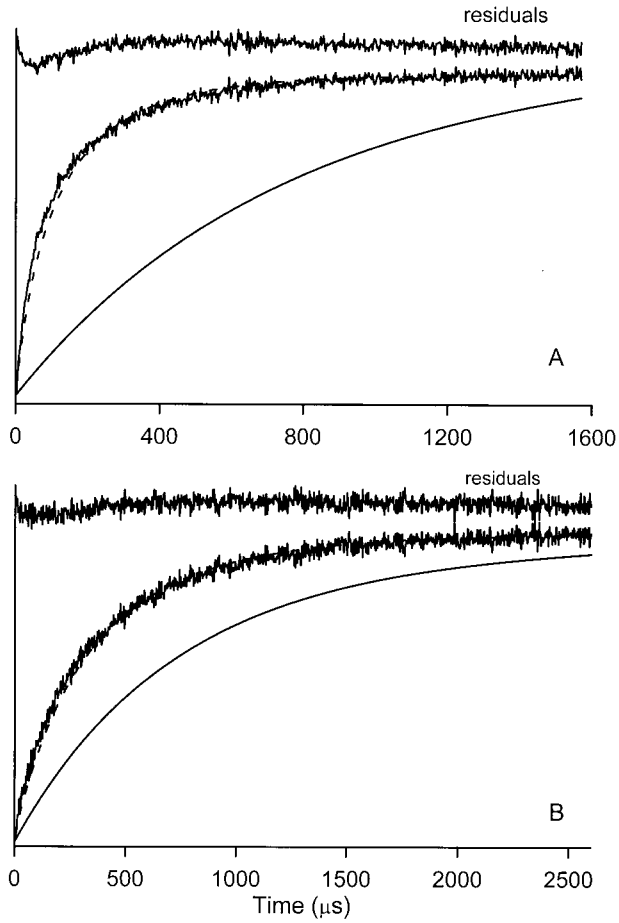

FIGURE 3 Saturation recovery curves for spin label in (*A*) 0.6 mM CN-metMbK98C-SL at 64 K and (*B*) 0.5 mM CN-metMbH12C-SL at 65 K in 1:1 buffer:glycerol. The dashed lines are simulated curves obtained with MENOSR for interspin distances of 20.5 Å (*A*) or 27.0 Å (*B*). The solid lines are the SR curves calculated for nitroxyl at the same temperatures in the absence of Fe(III), based on the fit function for which the parameters are given in the text. Differences between simulated and experimental values are plotted in the curves labeled residuals.

lations were performed in which it was assumed that the temperature at which the nitroxyl SR data were obtained was either higher or lower by 1 K than the temperature at which the values of T_1^0 and T_{1f} were obtained from the fit functions. The calculated deviations were about ± 0.5 Å, which is of the order of the experimental standard deviations, and suggests that uncertainties in temperature are a significant contribution to the standard deviations.

Analysis of results from Insight II simulations

Structures obtained by energy minimization and dynamic simulations were considered (Table 4). Due to the limited number of dynamics simulations and limited sampling, one cannot expect the sampled conformations to represent a Boltzmann distribution, so the calculated iron-nitroxyl distances were energy weighted using a Boltzmann distribution

$$\bar{R} = \frac{\sum_{i=1}^{800} R_i \times e^{-\Delta E_i/kT}}{\sum_{i=1}^{800} e^{-\Delta E_i/kT}},$$

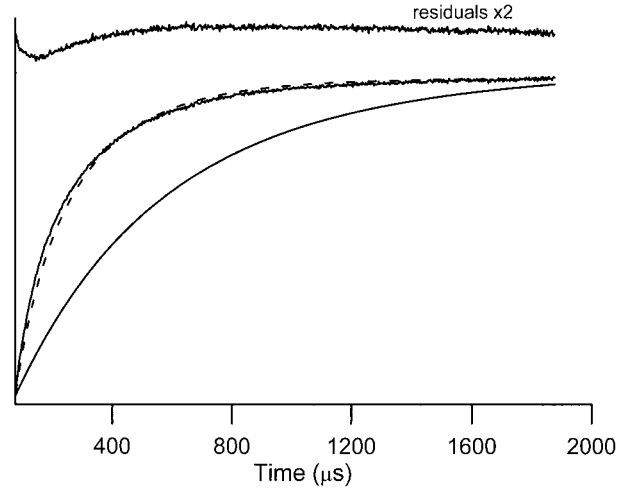

FIGURE 4 Saturation recovery curve for spin label in 0.6 mM Im-metMbK98C-SL at 77 K in 1:1 buffer:glycerol. The *dashed line* is the simulated curve obtained with MENOSR for an interspin distance of 16.3 Å. The *solid line* is the SR curve calculated for nitroxyl at the same temperature in the absence of Fe(III), based on the fit function for which the parameters are given in the text. Differences between simulated and experimental values are plotted on the curve labeled residuals.

where $\Delta E_i = E_i - E_{min}$. We also used $-\Delta E/10kT$ instead of $-\Delta E/kT$ in order to check the impact of other conformations with higher energies. The average distances were the same for both weighting methods and the spread was less than ± 1 Å for any data set.

To determine the orientation of the interspin vector relative to the heme axes, the origin of the coordinate system was moved to the iron and the *x, y, z*-axes were transformed. The transformed axes defined the iron-to-sixth-ligand direction as the *z* axis, the iron-to-a-ligating-N-of-heme as the *x* axis, and the direction perpendicular to the *x* and *z* axes as the *y* axis. The coordinates for the midpoint of the N-O bond of the nitroxyl radical were used to define the location of the unpaired electron. Each coordinated nitrogen was used, in succession, as the definition of the *x* axis, to obtain four sets of coordinates for angle calculation. These angles were averaged (Table 5). Uncertainties in angles reflect the irregularities in the structures: the heme plane is not perfectly planar, the four nitrogens ligated to the Fe are not at exactly the same distances, and the Fe is not precisely in the heme plane.

RESULTS AND DISCUSSION

The goal of this work is to use the effect of a rapidly relaxing low-spin or high-spin heme Fe(III) on the spin-lattice relaxation rate for a nitroxyl spin label to determine distances between the two paramagnetic centers in the range of 15 to 30 Å. The spin labels were attached to cysteines introduced into sperm whale myoglobin (Fig. 1). Surface locations were selected to minimize the effect of the label on the protein structure. Ligands were added to metMb and metMb-SL solutions to define the spin state of the iron. CN^- and Im (imidazole) form low-spin ($S = 1/2$) complexes and F^- and formate form high-spin ($S = 5/2$) complexes. Ligand concentrations were selected based on K_D

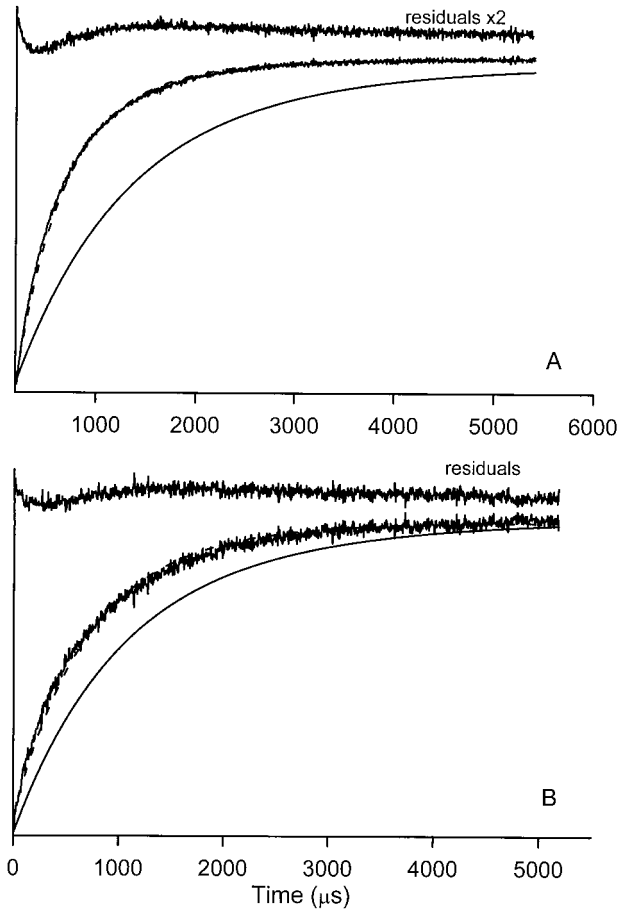

FIGURE 5 Saturation recovery curves for spin label in (*A*) 0.7 mM F-metMbV66C-SL at 55 K and (*B*) 0.7 mM F-metMbA53C-SL at 56 K in 1:1 buffer:glycerol. The *dashed lines* are simulated curves obtained with MENOSR for interspin distances of 18.5 Å (*A*) or 23.0 Å (*B*). The *solid lines* are the SR curves calculated for nitroxyl at the same temperatures in the absence of Fe(III), based on the fit function for which the parameters are given in the text. Differences between simulated and experimental values are plotted on the curves labeled residuals.

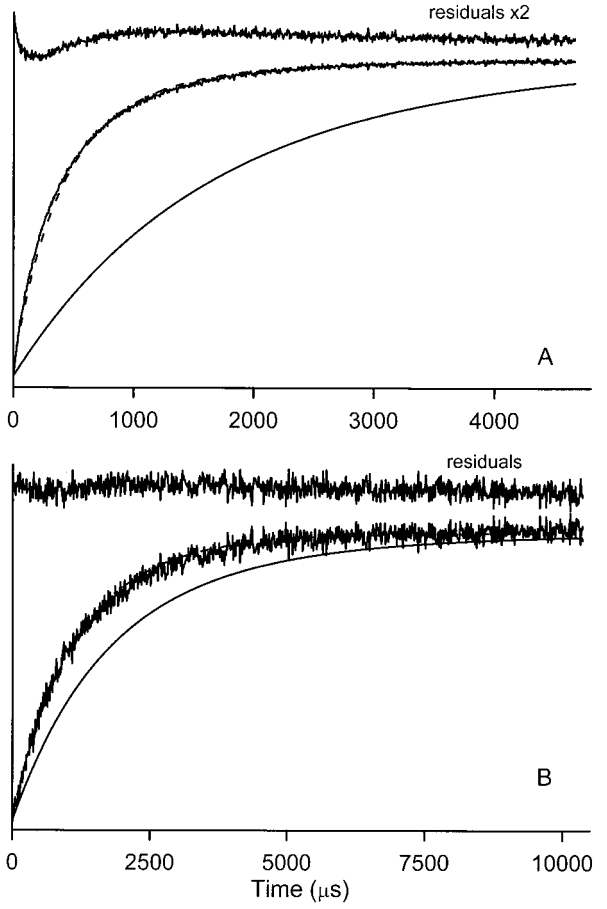

FIGURE 6 Saturation recovery curves for spin label in (*A*) 0.7 mM formate-metMbV66C-SL at 46 K and (*B*) 0.7 mM formate-metMbA53C-SL at 46 K in formate buffer:glycerol. The *dashed lines* are simulated curves obtained with MENOSR for interspin distances of 19.8 Å (*A*) or 26.5 Å (*B*). The *solid lines* are the SR curves calculated for nitroxyl at the same temperatures in the absence of Fe(III), based on the fit function for which the parameters are given in the text. Differences between simulated and experimental values are plotted in the curves labeled residuals.

values for horse heart myoglobin (Table 1). The goal was to achieve at least 97% conversion to the desired spin state.

CW EPR spectra

CW EPR spectra for characterization of the complexes were recorded at 15 K. At lower temperatures the spin-lattice relaxation rates for low-spin Fe(III) are so slow that it is difficult to record unsaturated spectra that are free of passage effects. Accurate CW spectra were necessary to estimate the relative proportions of high-spin and low-spin Fe(III) in the samples. The nitroxyl signal obscures the high-spin $g' = 2$ signal but does not interfere with the $g' = 6$ signal or with the g values for the low-spin iron, so the CW spectra for each of the spin-labeled variants provided useful quantitation of the iron spin states.

The g values obtained for CN-metMb and CN-metMb-SL were g_x (too broad to observe), $g_y = \sim 1.8–2.0$, and $g_z = 3.43$. They are similar to literature values for a single crystal of CN-metMb: $g_x = 0.93$, $g_y = 1.89$, $g_z = 3.45$ (Hori, 1971). For Im-metMb and Im-metMb-SL: $g_x = 1.55$, $g_y = 2.28$, $g_z = 2.90$, are similar to literature values for a single crystal of Im-metMb: $g_x = 1.72$, $g_y = 2.22$, $g_z = 2.80$ (Hori, 1971). The g values for the low-spin complexes are significantly different from those for OH-metMb, $g_x = 1.83$, $g_y = 2.14$, $g_z = 2.55$ (Magliozzo and Peisach, 1992), which confirms the coordination of the added ligands. The concentrations of high-spin species, presumably H_2O-metMb, present in the low-spin samples as determined by simulation of the CW spectra (Table 2) were typically less than ~5%, consistent with expectations of ligand binding based on the room temperature values of K_D.

TABLE 2 Iron-nitroxyl distances for low-spin complexes of metmyoglobin variants calculated from nitroxyl SR curves

Mb variant	−CN			−Imidazole		
	R (Å)	Temp (K)	h.s.%	R (Å)	Temp (K)	h.s.%
V66C	19.8 ± 0.8	16.3–172	3	16.9 ± 0.5	38–171	8
K98C	19.3 ± 1.3	16.2–168	2	15.8 ± 1.1	16.5–167	3
H12C	27.9 ± 1.9	30–118	5	–	–	–
A53C	30.4 ± 0.8	30–128	Low*	–	–	–

Uncertainties are the standard deviations of distances obtained at a series of temperatures within the range listed in the table.
*Low means not detectable in CW spectrum at 15 K.
h.s., high-spin.

High-spin complexes have distinctive $g'_x \cong g'_y \cong 6$ and $g'_z = 2$. The concentrations of low-spin species in the high-spin complexes ranged from about 10 to 30% (Table 3). These concentrations are higher than expected based on the ligand dissociation constants for F^-. The g values for the low-spin impurities in the F-metMb samples were g_x, 1.56–1.72; g_y, 2.21–2.23; g_z, 2.78–2.80 and, in formate-metMb, were g_x, 1.56; g_y, 2.14–2.23; g_z, 3.1, which are significantly different from OH-metMb. Based on the g values and on the variations between preparations of the same variant, we propose that the low-spin species are hemichromes formed by protein degradation (Bizzari and Cannistraro, 1993; DiIorio, 1981). It appears that strongly binding CN^- can largely convert reversibly formed hemichromes to the desired cyano complex (Table 2), but F^- and formate ligands do not bind tightly enough to compete effectively with hemichrome formation (Table 3). The UV-Vis spectra of the metMb-SL samples did not indicate the presence of hemichromes, which is consistent with literature reports (Arnold et al., 1999). Two kinds of metMb hemichromes have been reported (Arnold et al., 1999); a dihistidyl complex has $g_x = 1.53$, $g_y = 2.21$, $g_z = 2.97$, and a hydroxide derivative has $g_x = 1.83$, $g_y = 2.18$, $g_z = 2.59$. These g values suggest that the low-spin impurity in the high-spin samples is a dihistidyl hemichrome.

Differences between variants in the extent of hemichrome formation may be due to differences in stabilities of the variants. The first and rate-controlling step of autooxidation is the loss of oxygen from oxyMb (Brantley et al., 1993). Based on qualitative observations of the rate at which the Soret band shifted from 418 nm (oxyMb) to 409 nm (metMb) during sample preparation, the autooxidation rate is faster in all of the Mb variants examined than in wild-type Mb, and differs from variant to variant. The faster rates of autooxidation indicate that all of the variants are less stable than wild-type Mb. Conversion to the desired spin state tended to be more complete for the more stable variants metMbV66C and metMbK98C than for metMbH12C and metMbA53C. MetMbH12C is a very unstable variant, which may be related to the observation that spin-labeled His12 exhibits unusual pH-dependent changes in spin-label mobility (Postnikova, 1994). MbA53C dimerizes readily via disulfide formation, but this does not occur after spin-labeling. The presence of a mixture of iron spin states does not affect Fe T_2 measurements from CW line widths via simulation, since the high-spin and low-spin Fe signals are well separated. It can, however, affect calculations of the interspin distance based on the effect of iron on the nitroxyl relaxation.

Iron-nitroxyl interspin distances obtained from the nitroxyl SR curves

Low-spin Fe(III)

The iron-nitroxyl interspin distances obtained for the low-spin Fe(III) complexes of the spin-labeled myoglobin vari-

TABLE 3 Iron-nitroxyl distances for high-spin complexes of metmyoglobin variants calculated from nitroxyl SR curves

Mb variants	−F			−Formate		
	R (Å)	Temp (K)	l.s.%	R (Å)	Temp (K)	l.s.%
V66C	18.3 ± 0.6	16–162	Low*	21.6 ± 2.5	17–167	20
K98C	19	16–157	9	19	16–158	20
H12C(1)†	24.1 ± 0.8	45–75	18	29.8 ± 1.5	46–108	20
H12C(2)	24.5 ± 1.5	26–59	14	27.0 ± 0.4	26–57	29
A53C(1)	23.9 ± 2.4	36–75	13	28.7 ± 2.8	26–98	26
A53C(2)	25.9 ± 1.1	26–57	30	26.6 ± 1.2	26–57	29

Iron relaxation rates used in the calculations were obtained from the nitroxyl SR curves for F-metMbK98C-SL or formate-metMbK98C-SL with an interspin distance of 19 Å. Uncertainties are the standard deviations of distances obtained at a series of temperatures within the range listed in the table.
*Low means not detectable in CW spectra at 15 K.
†(1) and (2) refer to two replicate preparations of the Mb variant.
l.s., low-spin.

TABLE 4 Iron-nitroxyl interspin distances calculated with Insight (in Å)

Mb variants	Without solvent		With 5 Å water		With 10 Å glycerol		
	minimized	dynamics	minimized	dynamics	minimized	dynamics	Avg
V66C-H_2O	18.1	19.7	17.7	18.7	19.0	19.6	18.8
V66C-CN	18.9	20.9	17.0	18.4	17.0	18.2	18.4
V66C-Im	17.8	20.0	17.0	18.6	19.5	20.5	18.9
V66C-F	18.0	20.1	18.8	19.8	18.7	18.9	19.0
V66C-For	20.5	19.9	18.9	19.6	19.2	19.4	19.6
K98C-H_2O	17.3	16.3	17.8	17.3	18.1	18.5	17.6
K98C-Im	19.2	19.6	17.5	19.0	18.9	19.7	19.0
K98C-F	17.6	18.6	17.9	18.3	18.3	19.4	18.3
H12C-H_2O	33.0	32.7	29.8	31.0	31.9	31.7	31.7
H12C-CN	32.6	34.5	30.6	30.8	31.0	31.1	31.8
H12C-Im	31.4	33.4	33.5	33.7	31.7	32.1	32.6
H12C-F	31.2	32.8	30.7	31.5	30.1	32.3	31.4
H12C-For	32.5	33.5	29.0	30.3	32.9	30.2	31.4
A53C-H_2O	27.7	24.2	29.8	30.5	25.6	29.7	27.9
A53C-Im	26.2	28.5	28.0	29.4	28.1	29.2	28.2

Minimized refers to the energy-minimized structure and dynamics refers to the structure obtained by dynamic simulation, as defined in the Insight software. The iron-nitroxyl distance is defined as the average of Fe-to-N and Fe-to-O in the spin label.

ants by analysis of the nitroxyl SR curves using Eq. 2 are shown in Table 2. For the cyanide adducts the distances increased in the order V66C ~ K98C < H12C ~ A53C. The effect of the low-spin Fe(III) on the nitroxyl relaxation decreases as the distance is increased from 19 to 28 Å (Fig. 3) and significant effects are not expected at distances greater than about 30 Å for low-spin Fe(III) with relaxation rates comparable to those for CN-metMb. For approximately the same interspin distance the iron had a smaller impact on nitroxyl relaxation in Im-metMb-SL (Fig. 4) than in CN-metMb-SL (Fig. 3) because the relaxation rates for Fe(III) in Im-metMb are slower than in CN-metMb (Fig. 5 in Zhou et al., 1999). Interspin distances could not be obtained from the nitroxyl SR curves for Im-metMbH12C-SL or Im-metMbA53C-SL because of the small effect of the low-spin Fe(III) on the nitroxyl at the longer interspin distance of these variants. Systematically shorter interspin distances were obtained for the imidazole adducts of V66C and K98C than for the cyanide adducts. Since the axial ligand was not expected to have a large impact on the protein structure, these systematic differences were surprising.

High-spin Fe(III)

In our previous analyses of the effect of high-spin Fe(III) on nitroxyl SR curves we used Eq. 2 with the B term modified to include only the contribution from the $m_s = \pm 1/2$ tran-

TABLE 5 Orientation of interspin vector relative to heme axes calculated from structures generated with Insight

Mb variants	Without solvent		With 5 Å water		With 10 Å glycerol		Average	
	ε	θ	ε	θ	ε	θ	ε	θ
V66C-H_2O	56 ± 4.8	40 ± 3.0	66 ± 2.8	36 ± 0.8	59 ± 3.5	41 ± 8.5		
V66C-CN	62 ± 0.6	41 ± 0.5	56 ± 0.1	36 ± 0.1	50 ± 1.1	36 ± 0.4		
V66C-Im	61 ± 0.6	50 ± 0.3	63 ± 1.1	35 ± 0.5	57 ± 1.1	40 ± 0.6		
V66C-F	55 ± 1.0	49 ± 0.6	65 ± 1.6	35 ± 0.6	68 ± 0.4	33 ± 0.2		
V66C-For	65 ± 2.2	41 ± 0.5	63 ± 2.4	47 ± 1.2	52 ± 1.3	35 ± 1.2	60 ± 5	40 ± 5
K98C-H_2O	21 ± 2.1	26 ± 1.0	28 ± 2.5	16 ± 1.2	52 ± 3.2	15 ± 1.5		
K98C-Im	46 ± 0.1	16 ± 0.1	41 ± 1.3	11 ± 1.5	44 ± 0.8	10 ± 0.4		
K98C-F	30 ± 0.8	19 ± 0.4	41 ± 1.2	12 ± 0.5	39 ± 0.4	26 ± 0.5	38 ± 10	17 ± 6
H12C-H_2O	55 ± 1.6	91 ± 2.7	54 ± 1.5	77 ± 2.1	59 ± 2.6	95 ± 2.0		
H12C-CN	65 ± 0.6	87 ± 0.2	60 ± 1.2	82 ± 0.3	51 ± 0.1	86 ± 0.7		
H12C-Im	60 ± 0.1	91 ± 1.1	57 ± 0.6	82 ± 1.0	52 ± 0.6	81 ± 1.3		
H12C-F	56 ± 2.2	82 ± 1.5	51 ± 0.8	71 ± 1.6	65 ± 0.6	110 ± 0.3		
H12C-For	52 ± 2.5	90 ± 0.6	52 ± 1.7	72 ± 2.7	61 ± 0.1	85 ± 0.8	57 ± 5	85 ± 10
A53C-H_2O	18 ± 2.8	88 ± 13	12 ± 2.3	87 ± 22	14 ± 2.7	85 ± 12		
A53C-Im	26 ± 2.5	79 ± 8.5	12 ± 2.0	89 ± 16	25 ± 1.9	110 ± 5.1	18 ± 6	90 ± 11

ε = angle between interspin vector and the normal to the heme plane, θ = angle between the projection of the interspin vector on the heme plane and the x axis as defined by Hori (1971) and Sage (1997). Uncertainties reflect the deviations of the heme structure from a perfect plane.

sitions (Rakowsky et al., 1998; Seiter et al., 1998). The rationale was that because of the large zero-field splitting, ω_f - ω_s was so large for transitions involving $m_s = \pm 3/2$ or $\pm 5/2$ that the contributions from these transitions were negligible. We have now derived Eq. 3 in which the contributions from transitions with all values of m_s are included and the zero-field splitting is explicitly taken into account in the calculation of ω_f. Analysis of the nitroxyl SR curves for the high-spin spin-labeled variants using either the modification of Eq. 2 used previously (Rakowsky et al., 1998; Seiter et al., 1998), or Eq. 3 and the iron relaxation rates determined by analysis of the iron CW spectra for the $m_s = \pm 1/2$ transitions, gave interspin distances systematically shorter than those obtained for the low-spin adducts or from the Insight calculations described below.

New estimates of the high-spin Fe(III) relaxation rates were determined by setting the interspin distance for F-metMbK98C-SL and formate-metMbK98C-SL at 19 Å and adjusting the iron relaxation rates in Eq. 3 to fit the nitroxyl SR curves. The resulting iron relaxation rates are consistently faster than calculated from linewidths of the EPR-observable transitions (Fig. 2). These iron relaxation rates were then used with Eq. 3 to calculate the interspin distances for the other spin-labeled variants (Table 3). In effect, this procedure for the high-spin Fe(III) complexes obtains distances for other variants, relative to the assumed distance for the K98C variant. For both the fluoride and formate adducts the resulting interspin distances increased in the order V66C $<$ H12C $\sim$ A53C, although the distances for the fluoride adducts were systematically shorter than for the formate adducts. The iron relaxation rates for high-spin F-metMb are significantly slower than for formate-metMb throughout the temperature regime in which the effects of the iron on the nitroxyl relaxation rates were examined (Fig. 2). Because of the slower relaxation rates, the iron in the fluoride complexes has a smaller impact on the nitroxyl relaxation, for a given temperature and interspin distance, than the iron in the formate complexes (Figs. 5 and 6). The smaller effects of fluoride than of formate on the nitroxyl relaxation are expected to make the interspin distances calculated for the fluoride complexes more uncertain than for the formate complexes. However, the higher concentrations of hemichromes in most of the formate samples compared with the fluoride samples, could increase the uncertainties for the formate samples. To test the impact of low-spin hemichromes on the calculated interspin distances, results are compared for two preparations of the H12C and A53C variants (Table 3). In the second preparations efforts were made to decrease the total time required for protein purification, with the goal of decreasing hemichrome formation, but the impact on the hemichrome concentrations for most of the axial ligands was not large. The presence of low-spin hemichromes at concentrations of the order of 20% of the heme is likely to be a significant source of error. Work is in progress to prepare samples by another method with the goal of obtaining samples with lower hemichrome concentration.

Based on the larger value of S for high-spin Fe(III) than for low-spin Fe(III) it might have been anticipated that high-spin Fe(III) would have larger effects on the nitroxyl relaxation than low-spin Fe(III). Comparison of the saturation recovery curves for low-spin CN-metMbK98C-SL at 64 K (Fig. 3 *A*) and for high-spin formate-metMbV66C-SL at 57 K (Fig. 6 *A*) indicate comparable effects of the two Fe(III) spin states at similar interspin distances ($\sim$20 Å). The dominant reason why the high-spin iron is not more effective than low-spin iron in enhancing the nitroxyl relaxation rate is that in this temperature range low-spin Fe(III) relaxes faster than high-spin Fe(III) (Fig. 2). The maximum % change in nitroxyl relaxation rate due to interaction with low-spin CN-Fe(III) was observed at about 64 K, where the iron relaxation rate is about 5.8×10^9 s^{-1}. The maximum percentage change in nitroxyl relaxation rate for high-spin formate-Fe(III) complexes occurs at about 57 K, where the iron relaxation rate is about 3.0×10^8 s^{-1}. The relaxation rate for high-spin Fe(III) increases with increasing temperature more slowly than that of the non-interacting nitroxyl, so when viewed as a fractional change in the nitroxyl relaxation, the high-spin Fe(III) becomes less effective at higher temperatures. In addition, for most orientations of the molecules with respect to the external magnetic field, the denominator for the B term in Eq. 2 is substantially larger for high-spin Fe(III) than for low-spin Fe(III), which also diminishes the effectiveness of high-spin Fe(III) relative to low-spin Fe(III).

Iron-nitroxyl distances obtained from Insight simulations

Because of the many approximations used in modeling structures of large molecules, we examined several aspects of our calculations to test for reliability. All of our labeling sites are on the surface of the protein, so the 7- to 8-Å long spin label could be oriented in many different directions. Effects of solvation on geometries for the surface-exposed labels were of particular concern, so calculations were performed for three cases: without solvent, with a 5 Å water solvation shell, and with a 10 Å glycerol solvation shell. The SR data were obtained in 1:1 H_2O:glycerol solutions, but such a solvent box is at the limit of the software's capability, so the separate solvation models were used as an alternative. For the three models most of the calculated iron-nitroxyl distances fell within about ± 1 Å of the mean values (Table 4). Comparison of structures obtained by dynamic simulations indicated a variety of conformations with comparable energies, but these conformations result in similar iron-nitroxyl distances and orientations of the interspin vector relative to the heme axes (Table 5). Due to differences in local protein flexibility, there was a smaller range of iron-nitroxyl distances for the V66C and K98C

variants than for the H12C and A53C variants. The four heme ligands that were varied in SR experiments, and water, were modeled in V66C and H12C simulations, and several ligands were modeled for K98C and A53C, to examine effects of the ligand on interspin distances. Consistent with expectations, the calculated iron-nitroxyl distances were not strongly dependent upon the axial ligand (Table 4).

Comparison of interspin distances from Insight calculations and from nitroxyl SR data

Since the iron-nitroxyl distances calculated with Insight were not strongly dependent on solvation model or on axial ligand, the averages of values for various solvation models and axial ligands were calculated for each variant and are compared with the distances obtained from the SR data (Table 6). The distances between heme iron and the β-carbon of the naturally occurring amino acid at the mutation sites, calculated from the x-ray structures, are included in Table 6. Since the sites of the mutations are surface-exposed, the labels protrude into the solution and the iron-nitroxyl distances calculated with Insight are longer than Fe-C_β distances (Table 6). For the CN^- and formate adducts, the distances from the SR curves agree with each other and with the Insight results, within the estimated uncertainties. For L-metMbV66C-SL the interspin distances agree reasonably well for all ligands except imidazole. For the variants with longer distances, H12C and A53C, the distances obtained for the F^- adducts are systematically shorter than for the CN^- or formate complexes, or the Insight calculations, and seem unreasonably short relative to the Fe-C_β distances (Table 6). As discussed above, the effects of the iron on the nitroxyl relaxation rates are smaller for the Im and F^- complexes than for the CN^- and formate complexes. It appears that when the effects of the iron are smaller, the calculations tend to underestimate the interspin distance, which requires further investigation.

There also is greater variation in interspin distances at the longer distances, which may be due to several factors. 1) Distances of about 30 Å are near the upper limit for this technique for heme Fe(III) with relaxation rates comparable to those for CN-metMb and formate-metMb. Larger uncertainties are expected near the upper distance limits. 2) In this set of variants, the ones with the longer distances also are the less stable ones. The higher concentrations of hemichromes in samples of the less stable variants may contribute to greater uncertainty in the calculated distances. 3) The Insight calculations indicate that the H12C-SL and A53C-SL variants are more flexible than K98C-SL or V66C-SL, so the conformations of H12C-SL and A53C-SL may be more sensitive to concentrations of other species in solution than the conformations of K98C-SL and V66C-SL.

Another uncertainty in the calculations of interspin distance based on the nitroxyl SR curves is the orientation of the interspin vector relative to the axis of the heme. This is further complicated by the lack of agreement in the literature concerning the position of the principal g axes in the heme *x, y* plane. Although g_z is easily determined to be perpendicular to the heme plane, reported g_x orientations are as much as 40° away from each other (Hori, 1971; Shulman and Glarum, 1971; Sage, 1997). For high-spin Fe(III), this is less of a problem, as $g_x' \cong g_y' \cong 6.0$, and the orientation of the projection of the interspin vector on the heme plane does not affect our MENOSR simulations. Therefore, the only uncertainty in orientation for the high-spin Fe(III) is the angle between the interspin vector and heme *z* axis. For low-spin species, there is large g-anisotropy in the *x, y* plane, so both angles can affect our simulations. To determine the extent of such uncertainties, we used angles from the Insight simulations (Table 5) as well as random combinations of angles in the analysis of the SR curves. The variation in the interspin distances for high-spin species was ±0.5 Å at a distance of 24 Å for A53C-SL, which is well within the overall uncertainties of our experimental data. For the low-spin complexes the calculated interspin distances were more sensitive to the orientation of the interspin vector. For CN-metMbV66C-SL and Im-metMbV66C-SL the maximum variations in interspin distance over the range of relative orientations examined were 1.7 Å and 0.6 Å, respectively.

CONCLUSIONS

Interspin distances calculated by analysis of the effect of high-spin and low-spin heme Fe(III) on nitroxyl SR curves

TABLE 6 Comparison of interspin distances (Å) obtained from nitroxyl SR curves with Insight calculations

Ligand/ variant	CN^-	Imidazole	Formate	F^-	Insight, Fe-NO	Fe-C_β*
K98C	19.3 ± 1.3	15.8 ± 1.1	(19)†	(19)†	18.9 ± 1.0	11.1
V66C	19.8 ± 0.8	16.9 ± 0.5	21.6 ± 2.5	18.3 ± 0.6	18.3 ± 0.9	12.3
H12C	27.9 ± 1.9		28.4 ± 2.2	24.3 ± 1.1	31.8 ± 1.3	25.2
A53C	30.4 ± 0.8		27.8 ± 2.9	24.9 ± 2.1	28.1 ± 1.9	23.4

*Distance from iron to β-carbon of naturally occurring amino acid at this position, calculated from the X-ray crystal structure, Brookhaven pbd file pdb1mbw.

†Assumed distance used to determine high-spin Fe(III) relaxation rates that were then used in distance calculations for other variants with the same axial ligand.

for CN-metMb-SL and formate-metMb-SL were in reasonable agreement with each other and with distances obtained by Insight calculations for distances in the range of 18 to 30 Å. Distances were less reliable for imidazole and fluoride adducts, which is probably due to the slower relaxation rates for Im-metMb than for CN-metMb and of F-metMb than of formate metMb. Of the ligands examined, CN^- is the ligand of choice for the distance determinations because of tight ligand binding that provides uniformity of spin state, faster relaxation rates for the iron than when coordinated to other axial ligands, and the larger impact on nitroxyl relaxation rates over a wide temperature range. The upper limit for heme iron to nitroxyl distance measurements by these techniques is about 30 Å for iron relaxation rates similar to those in CN-metMb.

Partial support of this work by National Institutes of Health GM 21156 (to G. R. E. and S. S. E.) and GM57635 (to B. E. B.) is gratefully acknowledged.

REFERENCES

Aime, S., P. Ascenzi, M. Fasano, and S. Paoletti. 1993. NMR relaxometric studies of water accessibility to haem cavity in horse heart and sperm whale myoglobin. *Magn. Reson. Chem.* 31:S85–S89.

Aime, S., M. Fasano, S. Paoletti, F. Cutruzzolà, A. Desideri, M. Bolognesi, M. Rizzi, and P. Ascenzi. 1996. Structural determinants of fluoride and formate binding to hemoglobin and myoglobin: crystallographic and ^{1}H-NMR relaxometric study. *Biophys. J.* 70:482–488.

Antonini, E., and M. Brunori. 1971. Hemoglobin and Myoglobin in their Reactions with Ligands. North-Holland, Amsterdam. 44.

Arnold, E. V., D. S. Bohle, and P. A. Jordan. 1999. Reversible and irreversible hemichrome generation by the oxygenation of nitrosylmyoglobin. *Biochemistry.* 38:4750–4756.

Axup, A. W., M. Albin, S. L. Mayo, R. J. Crutchley, and H. B. Gray. 1988. Distance dependence of photoinduced long-range electron transfer in zinc/ruthenium-modified myoglobins. *J. Am. Chem. Soc.* 110:435–439.

Barnes, J. P., Z. Liang, H. S. Mchaourab, J. H. Freed, and W. L. Hubbell. 1999. A multifrequency electron spin resonance study of T4 lysozyme dynamics. *Biophys. J.* 76:3298–3306.

Berliner, L. J., and J. Reuben. 1989. Spin Labeling Theory and Applications. Biological Magnetic Resonance, vol. 8. Plenum Press, New York.

Biggin, M. D., T. J. Gibson, and G. F. Hong. 1983. Buffer gradient gels and ^{35}S label as an aid to rapid DNA sequence determination. *Proc. Natl. Acad. Sci. USA.* 80:3963–3965.

Bizzari, A. R., and S. Cannistraro. 1993. Solvent modulation of the structural heterogeneity in iron(III) myoglobin samples: a low temperature EPR investigation. *Eur. Biophys. J.* 22:259–267.

Bloembergen, N., S. Shapiro, P. S. Pershan, and J. O. Artman. 1959. Cross-relaxation in spin systems. *Phys. Rev.* 114:445–459.

Brantley, R. E. Jr., S. J. Smerdon, A. J. Wilkinson, E. W. Singleton, and J. S. Olson. 1993. The mechanism of autooxidation of myoglobin. *J. Biol. Chem.* 268:6995–7010.

Budker, V., J-L. Du, M. Seiter, G. R. Eaton, and S. S. Eaton. 1995. Electron-electron spin-spin interaction in spin-labeled low-spin methemoglobin. *Biophys. J.* 68:2531–2542.

Conti, E., C. Moser, M. Rizzi, A. Mattevi, C. Lionetti, A. Coda, P. Ascenzi, M. Brunori, and M. Bolognesi. 1993. X-ray crystal structure of *Aplysia limacina* myoglobin in different liganded states. *J. Mol. Biol.* 233: 498–508.

DiIorio, E. E. 1981. Preparation of derivatives of ferrous and ferric hemoglobin. *Methods Enzymol.* 76:57–72.

Dou, Y., J. S. Olson, A. J. Wilkinson, and M. Ikeda-Saito. 1996. Mechanism of hydrogen cyanide binding to myoglobin. *Biochemistry.* 35: 7107–7113.

Du, J-L., G. R. Eaton, and S. S. Eaton. 1995. Temperature, orientation, and solvent dependence of electron spin-lattice relaxation rates for nitroxyl radicals in glassy solvents and doped solids. *J. Magn. Reson.* 115: 213–221.

Eaton, S. S., and G. R. Eaton. 1988. Interactions of spin labels with transition metals. Part 2. *Coord. Chem. Rev.* 83:29–72.

Fann, Y.-C., J.-L. Ong, J. M. Nocek, and B. M. Hoffman. 1995. ^{19}F and ^{1,2}H ENDOR study of distal-pocket N(ϵ)-H$\cdot\cdot$F hydrogen bonding in fluorometmyoglobin. *J. Am. Chem. Soc.* 117:6109–6116.

Habeeb, A. F. S. A. 1972. Reaction of protein sulfydryl groups with Ellman's reagent. *Meth. Enzymol.* 25:457–464.

Hanania, G. I. H., A. Yeghiayan, and B. F. Cameron. 1966. Absorption spectra of sperm-whale ferrimyoglobin. *Biochem. J.* 98:189–192.

Hirsch, D. J., and G. W. Brudvig. 1993. Long-range electron spin-spin interactions in the bacterial photosynthetic reaction center. *J. Phys. Chem.* 97:13216–13222.

Hori, H. 1971. Analysis of the principal g-tensors in single crystals of ferrimyoglobin complexes. *Biochim. Biophys. Acta.* 251:227–235.

Hubbell, W. L., and C. Altenbach. 1994. Investigation of structure and dynamics in membrane proteins using site-directed spin labeling. *Curr. Opin. Struct. Biol.* 4:566–573.

Kulikov, A. V., and G. I. Likhtenshtein. 1977. The use of spin relaxation phenomena in the investigation of the structure of model and biological systems by the method of spin labels. *Adv. Mol. Relax. and Interact. Proc.* 10:47–69.

Leci, E., A. Brancaccio, F. Cutruzzolà, C. T. Allocatelli, C. Tarricone, M. Bolognesi, A. Desideri, and P. Ascenzi. 1995. Formate binding to ferric wild type and mutant myoglobins, thermodynamic and X-ray crystallographic study. *FEBS Lett.* 357:227–229.

Leonard, J. J., T. Yonetani, and J. B. Callis. 1974. A fluorescence study of hybrid hemoglobins containing free base and zinc protoporphyrin IX. *Biochemistry.* 13:1460–1464.

Lionetti, C., M. G. Guanziroli, F. Frigerio P. Ascenzi, and M. Bolognesi. 1991. X-ray structure of the ferric sperm whale myoglobin: imidazole complex at 2.0 Å resolution. *J. Mol. Biol.* 217:409–412.

Magliozzo, R. S., and J. Peisach. 1992. Electron spin echo envelope modulation spectroscopic study of iron-nitrogen interactions in myoglobin hydroxide and Fe(III) tetraphenylporphyrin models. *Biochemistry.* 31:189–199.

Maniatis, T., E. F. Fritsch, and J. Sambrook. 1992. Molecular Cloning: A Laboratory Manual. Cold Spring Harbor Laboratory Press, Cold Spring Harbor, NY.

Manoharan, P. T., J. T. Wang, K. Alston, and J. M. Rifkind. 1990. Spin label probes of the environment of cysteine β-93 in hemoglobin. *Hemoglobin.* 14:41–67.

Mansy, S. S., J. S. Olson, G. Gonzalez, and M. A. Gilles-Gonzalez. 1998. Imidazole is a sensitive probe of steric hindrance in the distal pockets of oxygen-binding heme proteins. *Biochemistry.* 37:12452–12457.

Martin, R. E., M. Pannier, F. Diederich, V. Gramlich, M. Hubrich, and H. W. Spiess. 1998. Determination of end-to-end distances in a series of TEMPO diradicals of up to 2.8 nm length with a new four-pulse double electron electron resonance experiment. *Angew. Chem.* 37:2834–2837.

Milov, A. D., A. G. Marysov, and Yu. D. Tsvetkov. 1998. Pulsed electron double resonance (PELDOR) and its application in free radicals research. *Appl. Magn. Reson.* 15:107–143.

Oganesyan, V. S., and Y. A. Sharonov. 1998. Determination of zero-field splitting and evidence for the presence of charge-transfer transitions in the Soret region of high-spin ferric hemoproteins obtained from an analysis of low-temperature magnetic circular dichroism. *Biochim. Biophys. Acta.* 1429:163–175.

Phillips, G. N., Jr., R. M. Arduini, B. A. Springer, and S. G. Sligar. 1990. Crystal structure of myoglobin from a synthetic gene. *Proteins: Struct. Funct. Genet.* 7:358–365.

Poole, C. P., Jr., and H. Farach. 1971. Relaxation in Magnetic Resonance. Academic Press, New York. 70–71 and 196–200.

Postnikova, G. B. 1994. Chemical modification of myoglobin by isothiocyanate reagents: effect of N-terminal amino group modification on protein conformation. *Biochemistry (Moscow).* 59:1069–1075.

Quine, R. W., S. S. Eaton, and G. R. Eaton. 1992. A saturation recovery electron paramagnetic resonance spectrometer. *Rev. Sci. Instrum.* 63: 4252–4262.

Rabenstein, M. D., and Y. K. Shin. 1995. Determination of the distance between two spin labels attached to a macromolecule. *Proc. Natl. Acad. Sci. USA.* 92:8239–8243.

Rakowsky, M. H., K. M. More, A. V. Kulikov, G. R. Eaton, and S. S. Eaton. 1995. Time-domain electron paramagnetic resonance as a probe of electron-electron spin-spin interaction in spin-labeled low-spin iron porphyrins. *J. Am. Chem. Soc.* 117:2049–2057.

Rakowsky, M. H., A. Zecevic, G. R. Eaton. and S. S. Eaton. 1998. Determination of high-spin iron(III) distances in spin-labeled porphyrins by time-domain EPR. *J. Magn. Reson.* 131:97–110.

Rubenstein, M., A. Baram, and Z. Luz. 1971. Electronic and nuclear relaxation in solutions of transition metal ions with spin S = 3/2 and 5/2. *Mol. Phys.* 20:67–80.

Russel, M., S. Kidd, and M. R. Kelley. 1986. An improved filamentous helper phage for generating single-stranded plasmid DNA. *Gene.* 45: 333–338.

Sage, J. T. 1997. Infrared crystallography: structural refinement through spectroscopy. *Appl. Spectros.* 51:568–573.

Scholes, C. P., R. A. Isaacson, and G. Feher. 1971. Determination of the zero-field splitting of Fe^{3+} in heme proteins from the temperature dependence of the spin-lattice relaxation rate. *Biochim. Biophys. Acta.* 244:206–210.

Scholler, D. M., M.-Y. R. Wang, and B. M. Hoffman. 1978. Metal-substituted hemoglobin and other hemoproteins. *Meth. Enzymol.* 52: 487–493.

Seiter, M., V. Budker, J.-L. Du, G. R. Eaton, and S. S. Eaton. 1998. Interspin distances determined by time domain EPR of spin-labeled high-spin methemoglobin. *Inorg. Chim. Acta.* 273:354–366.

Shulman, R. G., and S. H. Glarum. 1971. Electronic structure of cyanide complexes of hemes and heme proteins. *J. Mol. Biol.* 57:93–115.

Springer, B. A., and S. G. Sligar. 1987. High-level expression of sperm whale myoglobin in *Escherichia coli*. *Proc. Natl. Acad. Sci. USA.* 84:8961–8965.

Stryer, L. J. 1965. The interaction of a naphthalene dye with apomyoglobin and apohemoglobin, a fluorescent probe of non-polar binding sites. *J. Mol. Biol.* 13:482–495.

Teale, F. W. J. 1959. Cleavage of the haem-protein link by acid methylethylketone. *Biochim. Biophys. Acta.* 35:543.

Zecevic, A., G. R. Eaton, S. S. Eaton, and M. Lindgren. 1998. Dephasing of electron spin echoes for nitroxyl radicals in glassy solvents by non-methyl and methyl protons. *Mol. Phys.* 95:1255–1265.

Zhou, Y., B. E. Bowler, G. R. Eaton, and S. S. Eaton. 1999. Electron spin-lattice relaxation rates for S = 1/2 molecular species in glassy matrices or magnetically dilute solids at temperatures between 10 and 300 K. *J. Magn. Reson.* 139:165–174.

Zhou, Y., B. E. Bowler, G. R. Eaton, and S. S. Eaton. 2000. Electron spin-lattice relaxation rates for high-spin Fe(III) in glassy solvents at temperatures between 6 and 298 K. *J. Magn. Reson.* 144:115–122.

Zuniga, E. H., and B. T. Nall. 1983. Folding of yeast iso-1-AM cytochrome *c. Biochemistry.* 22:1430–1437.